Dynamics of strongly localized Lyapunov vectors in many-hard-disk systems

Tooru Taniguchi and Gary P. Morriss
School of Physics, University of New South Wales, Sydney, New South Wales 2052, Australia
(Received 28 June 2005; published 14 March 2006)

The dynamics of the localized region of the Lyapunov vector for the largest Lyapunov exponent is discussed in quasi-one-dimensional hard-disk systems at low density. We introduce a hopping rate to quantitatively describe the movement of the localized region of the Lyapunov vector, and show that it is a decreasing function of the hopping distance, implying a spatial correlation of the localized regions. This behavior is explained quantitatively by a brick accumulation model derived from hard-disk dynamics in the low density limit, in which hopping of the localized Lyapunov vector is represented as the movement of the highest brick position. We also give an analytical expression for the hopping rate, which is obtained as a sum of probability distributions for brick height configurations between two separated highest brick sites. The results of these simple models are in good agreement with the simulation results for hard-disk systems.

DOI: 10.1103/PhysRevE.73.036208 PACS number(s): 05.45.Jn, 05.45.Pq, 02.70.Ns, 05.20.Jj

I. INTRODUCTION

The dynamical instability and many-body nature play essential roles in the justification of a statistical treatment for deterministic dynamical systems. The dynamical instability is described as a rapid expansion of the difference between two nearby trajectories, namely the Lyapunov vector. A system is called chaotic if at least one exponential rate of change of the amplitude of the Lyapunov vector (Lyapunov exponent) is positive. A Lyapunov exponent λ is defined for each independent direction of the phase space, so the chaotic properties of many-body systems can be characterized by an ordered set of Lyapunov exponents, the so-called Lyapunov spectrum $\{\lambda^{(1)},\lambda^{(2)},\ldots\}$ where $\lambda^{(1)}\geqslant\lambda^{(2)}\geqslant\ldots$. The Lyapunov spectrum is connected to the contraction rate of the phase space volume (roughly speaking, the dissipation rate) through the sum of all the Lyapunov exponents, allowing the calculation of transport coefficients from the Lyapunov spectra [1–3]. The conjugate pairing rule for Lyapunov spectra for Hamiltonian systems and some uniformly thermostated systems (e.g., isokinetic Gaussian thermostat) reduces the calculation of the sum of all the Lyapunov exponents to the sum of just one pair [4–7]. The set of all positive Lyapunov exponents specifies the natural invariant measure [8,9]. Representations of the invariant measure can be calculated from the Lyapunov exponents of periodic orbits [10] and these ideas motivated the earliest fluctuation theorem [11–13]. On the other hand, recently, much attention has been paid to individual Lyapunov exponents and their Lyapunov vectors for many-body systems. As each Lyapunov exponent has the dimensions of inverse time, the Lyapunov spectrum can be regarded as a time-scale spectrum. From this point of view, Lyapunov exponents with small absolute values are connected to large and macroscopic time-scale behavior of many-body systems, and in this region the wavelike structure of Lyapunov vectors, known as the Lyapunov modes, is observed [14–18]. The Lyapunov mode is a reflection of a collective movement (phonon mode) of many-body systems, and comes from dynamical conservation laws and translational invariance [18–21]. On the other hand, the large Lyapunov exponents are dominated by small and microscopic time-scale movement, and in this region the spatially localized behavior of the Lyapunov vector, the so-called Lyapunov localization, appears [22–29]. Analytical calculations have been attempted for the largest Lyapunov exponent of many-body chaotic systems, and even for the full Lyapunov spectra in some cases [15,26,30–37]. The time-scale separation in many-body systems is crucial to extract a macroscopic dynamics from microscopic many-body dynamics, and the Lyapunov spectrum allows us to discuss it dynamically.

One of the features of Lyapunov vectors for many-body systems is Lyapunov localization, which appears when the components of a few particles dominate the Lyapunov vector. This strongly localized region of a Lyapunov vector moves with time. The magnitude of the localization of each Lyapunov vector can be measured quantitatively by the Lyapunov localization spectrum, which is defined as a set of exponential functions of entropylike quantities for the normalized amplitudes of the Lyapunov vector components [29,38,39]. We have previously reported that the Lyapunov localization spectra show a critical bending point at low density, and this limits the number of strongly localized Lyapunov vectors. At the bending point the dependence of the Lyapunov localization spectrum with respect to Lyapunov indices changes from linear to exponential [29,38]. This critical bending point behavior of the Lyapunov localization spectrum appears when kinetic theory properties (e.g., the Krylov relation for the largest Lyapunov exponent, and the mean free time being inversely proportional to density, etc.) dominate the behavior of the hard-disk system. However, the Lyapunov localization spectrum requires a time-average and characterizes only the static localization of the Lyapunov vectors. The physical meaning of the movement of the localized regions of Lyapunov vectors is not clearly understood.

The principal aim of this paper is to study dynamically the movement of the localized region of the Lyapunov vectors corresponding to the largest exponent in hard-disk systems at low density. To discuss this problem we use the fact that at low density only that part of the Lyapunov vector corre-

sponding to two particles is large [29]. This is observed numerically for the Lyapunov vectors corresponding to exponents in the linear dependence region of the Lyapunov localization spectrum. At low density, this is due to the fact that collisions are rare and typically occur between only two particles. The movement of the localized region of the Lyapunov vector appears to be a series of jumps or hops, so we introduce a hopping rate to describe the dynamics. To simplify the problem we consider quasi-one-dimensional systems, in which the system width is so narrow that disks always remain in the same order [18,21,29,38] and we limit our study to the largest exponent. We show that the hopping rate depends inversely on the distance. This implies that there is some spatial correlation among localized regions of Lyapunov vectors.

We explain the hopping-distance dependence of the hopping rate in many-hard-disk systems in two ways. First we use a simple model expressed as an accumulation of bricks. Here, the hopping of the localized region of the Lyapunov vectors is expressed as a change in the position of the highest brick site. This model is a one-dimensional version of the so-called clock model, which has been used to calculate Lyapunov exponents for many-hard-disk systems [35–37]. We demonstrate that this model can reproduce the largest Lyapunov exponent for the quasi-one-dimensional hard-disk system. As a second approach to the hopping behavior we propose an analytical method to calculate the hopping rate from the sum of probability distributions for the brick height configurations between two separated highest brick sites. Using this analytical approach we can also discuss the relation between the hopping rate and the Lyapunov exponent. Hopping rates calculated by these two approaches are in good agreement with the ones for quasi-one-dimensional hard-disk systems.

The outline of this paper is as follows. In Sec. II we introduce the quasi-one-dimensional hard-disk system and show the localized behavior of the Lyapunov vector corresponding to the largest Lyapunov exponent at low density. In Sec. III we introduce the hopping rate of the localized region of the Lyapunov vectors and show the hopping-distance dependence for many-hard-disk systems. In Sec. IV we discuss the hopping rate using a brick accumulation model. In Sec. V we propose an analytical expression for the hopping rate. Section VI is our conclusion and some remarks. In Appendix A we discuss the technical details of the calculation of the hopping rate. In Appendix B we give a microscopic derivation of the brick accumulation model.

II. QUASI-ONE-DIMENSIONAL SYSTEM AND LOCALIZATION OF LYAPUNOV VECTORS

The system we consider in this paper is a quasi-one-dimensional system consisting of N hard-disks in periodic boundary conditions. All of the particles are identical with radius R and mass M, and the shape of the system is rectangular with the length L_x and the width L_y satisfying the inequality $2R<L_y<4R$. The schematic illustration of the system is given in Fig. 1, in which we number particles $1,2,\ldots,N$ from left to right. For the actual numerical results

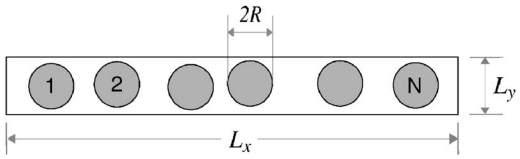

FIG. 1. A quasi-one-dimensional system consisting of hard-disks with radius R. The length L_x and the width L_y of the system control the density. The width L_y satisfies the inequality $2R<L_y<4R$, so that the disks remain in the same order and particles can be numbered $1,2,\ldots,N$ from left to right.

shown in this paper, we used: $R=1$, $M=1$, the total energy of the system $E=N$, the system width $L_y=2R(1+10^{-6})$, and the system length $L_x=NL_y(1+d)$ with the constant d controlling the density $\rho\equiv N\pi R^2/(L_xL_y)$. In the quasi-one-dimensional system, the particle interactions are restricted to nearest-neighbor particles only, so particles remain in the same order. These features require less calculation effort and a simpler representation of results for the quasi-one-dimensional system compared with fully two-dimensional systems. The quasi-one-dimensional system has already been used to investigate the localized behavior of Lyapunov vectors [29,38], the wavelike structure of Lyapunov vectors [18,19,21], and the transition between quasi-one-dimensional and fully two-dimensional systems [40].

The dynamics of Lyapunov vectors in many-hard-disk systems is well established, and readers should refer to the references, for example, Ref. [45], for more detailed discussions. In many-hard-disk systems the dynamics is separated into a free-flight part and a collision part, and the free-flight part of the dynamics is integrable. This property allow us to express the dynamical evolution as a simple multiplication of time-evolutional matrices for the free-flight and the collision, leading to a fast and more accurate numerical simulation than for soft-core interaction models. For numerical calculations of the Lyapunov vectors shown in this paper, we use the algorithm developed by Benettin *et al.* [41] and Shimada and Nagashima [42] (also see Refs. [43,44]). This algorithm is characterized by intermittent (e.g., after every collision) reorthogonalization and renormalization of Lyapunov vectors, preventing a divergence of the amplitude.

We use the notation $\delta\mathbf{\Gamma}^{(n)}(t)\equiv[\delta\mathbf{\Gamma}_1^{(n)}(t),\delta\mathbf{\Gamma}_2^{(n)}(t),\ldots,\delta\mathbf{\Gamma}_N^{(n)}(t)]$ for the Lyapunov vector corresponding to the nth Lyapunov exponent $\lambda^{(n)}$ at time t. Here, $\delta\mathbf{\Gamma}_j^{(n)}(t)$ is the Lyapunov vector component contributed by the jth particle in the nth Lyapunov exponent at time t. To express the localized behavior of the Lyapunov vectors we introduce the quantity $\gamma_j^{(n)}(t)$ as

$$\gamma_j^{(n)}(t)\equiv\frac{|\delta\mathbf{\Gamma}_j^{(n)}(t)|^2}{\sum_{k=1}^{N}|\delta\mathbf{\Gamma}_k^{(n)}(t)|^2}, \tag{1}$$

which is the normalized amplitude of the Lyapunov vector component for the jth particle for the nth Lyapunov exponent $\lambda^{(n)}$ at time t. Strongly localized behavior of the Lyapunov vector occurs when only a few of the $\gamma_j^{(n)}(t)$, $j=1,2,\ldots,N$

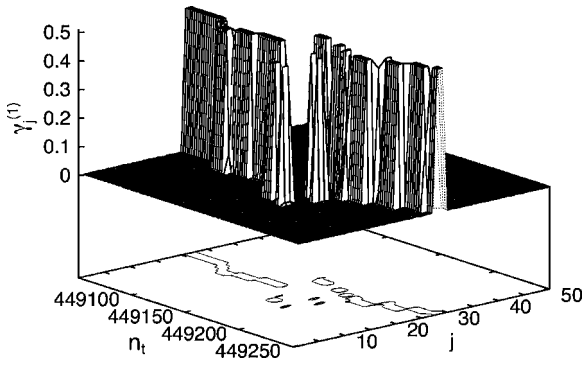

FIG. 2. The normalized amplitude $\gamma_j^{(1)}$ of the Lyapunov vector particle component corresponding to the largest Lyapunov exponent as a function of the collision number n_t and the particle index j in a quasi-one-dimensional hard-disk system with $d=10^5$ and $N=50$. On the base of this graph is a contour plot of $\gamma_j^{(1)}$ at the level 0.2.

contribute significantly, as in Fig. 2. Here a graph of the normalized amplitude $\gamma_j^{(1)}$ of the Lyapunov vector components for the jth particle, corresponding to the largest Lyapunov exponent $\lambda^{(1)}$, are plotted as functions of the particle index j and the collision number n_t ($\approx t/\tau$ with time t and the mean free time τ). The system is quasi-one-dimensional consisting of 50 hard disks with $d=10^5$ (the density $\rho \approx 7.85 \times 10^{-6}$). From this figure we recognize that the significant components of the Lyapunov vector are concentrated at two nearest-neighbor particles. This is characteristic of hard-disk systems at low density and for large Lyapunov exponents in the linear region of the Lyapunov localization spectrum [29,38].

We observe that such localized regions of the Lyapunov vector move with time in discrete jumps or hops, in Fig. 2. This characteristic hopping has already been shown in Ref. [29] and that such hopping of the significant components of $\gamma_j^{(n)}(t)$ is connected with particle collisions. However, not every collision causes the localized region of the Lyapunov vector to move. In this sense, particle collisions themselves are not sufficient to explain the hopping movement of the Lyapunov localization. In this paper for simplicity we consider only the Lyapunov vector $\delta\mathbf{\Gamma}^{(1)}$ corresponding to the largest Lyapunov exponent $\lambda^{(1)}$.

III. HOPPING RATE OF LOCALIZED LYAPUNOV VECTORS

An advantage of the quasi-one-dimensional system in investigations of Lyapunov localization is that the movement of particles in the transverse direction are suppressed, and roughly speaking, the particle number corresponds to the particle's position. Noting this we describe the hopping behavior of spatially localized Lyapunov vectors as the hopping of particle indices whose $\gamma_j^{(n)}$ defined by Eq. (1) have large values.

As shown in Refs. [29,38] the particle indices with a large value of $\gamma_j^{(1)}$ are a pair of nearest-neighbor particles in the low density limit, and we can introduce the hopping distance h as the change of particle indices. In this definition the

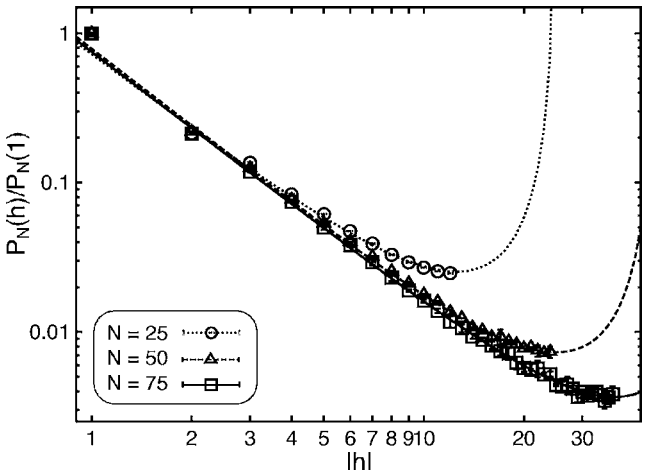

FIG. 3. The normalized hopping rates $P_N(h)/P_N(1)$ for quasi-one-dimensional systems of different sizes at the same density ($d=10^3$) as a function of the hopping distance $|h|$. The number of particles is $N=25$ (circles), 50 (triangles), and 75 (squares). The graphs are log-log plots with error bars are given by $|P_N(h)-P_N(-h)|/P_N(1)$. The lines are fits of the numerical data to functions based on Eq. (2) with power functions as the asymptotic form of the hopping rate.

hopping distance h is an integer satisfying $-[N/2] \leqslant h \leqslant [N/2]$, where $[x]$ is the integer part of the real number x. It should also be noted that we take the particle index j to be equivalent to the index $j \pm N$, because of periodic boundary conditions, so a hopping distance $h \pm N$ is equivalent to h. More technical details of the calculation of the hopping distance h are given in Appendix A. Using this hopping distance h, in numerical simulations, we count the number $\mathcal{N}_T(h)$ of hops with hopping distance h in a time-interval T, and we can define the hopping rate $P_N(h)$ as a function $\mathcal{N}_T(h)/T$ as $T \to \infty$, namely the average number of hops with a hopping distance per unit time. For actual data shown in this paper, we use the hopping rate $P_N(h)/P_N(1) = \lim_{T\to\infty} \mathcal{N}_T(h)/\mathcal{N}_T(1)$ normalized by $P_N(1)$. From the reflection symmetry of the quasi-one-dimensional system in the longitudinal direction, the hopping rate $P_N(h)$ must be symmetric, namely $P_N(h) = P_N(-h)$. We use this hopping rate to quantitatively discuss the hopping dynamics for localized Lyapunov vectors.

Figure 3 shows log-log plots of the normalized hopping rates as a function of $|h|$ for different numbers of particles. Noting the symmetry property $P_N(-h)=P_N(h)$, we use $|P_N(h)-P_N(-h)|/P_N(1)$ as error bars in Fig. 3. Clearly, from Fig. 3, the hopping rate $P_N(|h|)$ decreases as $|h|$ increases, implying spatial correlation between the localized regions of a Lyapunov vector, rather than random hopping.

The *turn-up* in the tail of the normalized hopping rate $P_N(h)/P_N(1)$ in Fig. 3 can be explained as an effect of periodic boundary conditions. Under periodic boundary conditions the hopping distance $h+jN$ for any integer j is observed as the hopping distance h in the quasi-one-dimensional system consisting of N hard disks. Therefore using the hopping rate $P_\infty(h)$ in the thermodynamics limit ($N \to \infty$ at a fixed density) the hopping rate $P_N(h)$ for a finite system should be represented as

TABLE I. Fitting parameters for the function $f(h)$ shown in Fig. 3 assuming that $P_\infty(h) \propto |h|^{-\beta}$ for quasi-one-dimensional systems of different numbers of particles N but the same density. The coefficients α and β are essentially independent of N.

N	α	β
25	0.72±0.04	1.67±0.03
50	0.79±0.02	1.72±0.01
75	0.75±0.02	1.71±0.01

$$P_N(h) = \sum_{j=-\infty}^{\infty} P_\infty(h + jN) \tag{2}$$

for $h=-[N/2],-[N/2]+1,\ldots,[N/2]$. The terms on the right-hand side of Eq. (2) with $j \neq 0$ cause the *turn-up* in the tail of the hopping rate $P_N(h)$ for a finite system. In this sense we can explain the N-dependence of the hopping rate $P_N(h)$ using the distribution $P_\infty(h)$. To demonstrate this we fitted the numerical data for $P_N(h)/P_N(1)$ shown in Fig. 3 to the function $f(h) \equiv \alpha \Sigma_{j=-2}^{2} |h+jN|^{-\beta}$ assuming a power law decay of $P_\infty(h) \propto |h|^{-\beta}$ with fitting parameters α and β, neglecting the terms for $|j| \geqslant 3$. Here, the fits are a dotted line for $N=25$, a broken line for $N=50$, and a solid line for $N=75$. Note that these sets (α,β) of fitting parameters in Table I are almost independent of the number of particles N. As shown in Fig. 3, these fitting lines nicely reproduce the values of the numerical data, especially the *turn-ups*.

In Appendix A we show that the normalized hopping rate $P_N(h)/P_N(1)$ is almost density-independent at least for $10^3 < d < 10^5$ (that is, $7.85\times10^{-6} < \rho < 7.85\times10^{-4}$). However, as the density decreases there is a subtle increase in the normalized hopping rate, associated with a decrease in the parameter β.

IV. BRICK ACCUMULATION MODEL

The hopping rate of the localized region of the Lyapunov vector is spatially correlated. We explain this characteristic using a simple one-dimensional model, which we call the *brick accumulation model*. In Appendix B we give a full derivation of the brick model, but here we give a brief outline of the argument. Considering the phase space perturbation at low density $\rho \ll 1$, the change between collisions is given by Eqs. (B23) and (B24), that is

$$\delta\mathbf{\Gamma}_j(t_n^+) \sim \tau_n \delta\Xi^{[n-1]} \sim -\delta\mathbf{\Gamma}_{j+1}(t_n^+) \tag{3}$$

to leading order in the time between collisions τ_n. Here, $\delta\Xi^{[n-1]}$ is independent of τ_n and is connected to the Lyapunov vector at t_{n-1}^+ just after the $(n-1)$th collision. It follows that after collision $|\delta\mathbf{\Gamma}_j(t_n^+)| = |\delta\mathbf{\Gamma}_{j+1}(t_n^+)|$ so the contributions from the two colliding particles j and $j+1$ are equal. We introduce a brick height $\mathcal{K}_l(n)$ for the lth particle after the nth collision and define the change between collision $n-1$ and collision n to be

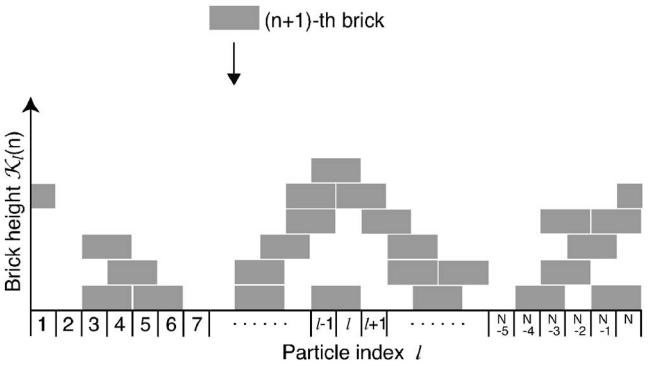

FIG. 4. The brick accumulation model expressing the dynamics of the amplitude of the Lyapunov vector components for each particle in a quasi-one-dimensional system.

$$\Delta\mathcal{K}_l(n) \equiv -\frac{1}{\ln\rho} \ln \frac{|\delta\mathbf{\Gamma}_l(t_n^+)|}{|\delta\mathbf{\Gamma}_l(t_{n-1}^+)|}. \tag{4}$$

We interpret the contribution from each collision as adding an amount $-\Delta\mathcal{K}_j(n)\ln\rho$ to each of the $\ln|\delta\mathbf{\Gamma}|$'s of the colliding particles. One of the colliding particles initial contribution will dominate the other, so we add the collisional change to the dominant particle and then synchronize the contribution for the other particle. Thus the dynamics of the brick model reduces to the following rule for the evolution of the brick height $\mathcal{K}_l(n)$:

$$\mathcal{K}_l(n) = \begin{cases} \max\{\mathcal{K}_j(n-1), \mathcal{K}_{j+1}(n-1)\} + 1 & \text{if } l \in \{j, j+1\} \\ \mathcal{K}_l(n-1) & \text{if } l \notin \{j, j+1\}, \end{cases} \tag{5}$$

namely $\Delta\mathcal{K}_l(n) = \max\{\mathcal{K}_j(n-1), \mathcal{K}_{j+1}(n-1)\} + 1 - \mathcal{K}_l(n-1)$ if $l \in \{j, j+1\}$, and $=0$ otherwise.

A schematic illustration of the brick model is given in Fig. 4. It is a one-dimensional model with N sites in the horizontal direction. The bricks are dropped at random and occupy a pair of neighboring sites. Each brick has width 2 and height 1 and they accumulate at sites without overlap. The dynamics of the brick model is described using the brick height $\mathcal{K}_j(n)$ by Eq. (5). The total brick height $\mathcal{K}_j(n)$ takes on integer values and the colliding particles are j and $j+1$ where j is chosen randomly.

The brick accumulation model is a one-dimensional version of the so-called *clock model* [35–37], which has been used to calculate the Lyapunov exponents for many-hard-disk systems. In the clock model, the brick height $\mathcal{K}_l(n)$ is called the *clock value* of the lth particle after the nth collision, and the dynamics (5) is expressed as an adjustment of the clock values of colliding particles. In the one-dimensional case it is easy to visualize the accumulation of bricks which is essential for the analytical approach to the hopping rate discussed in Sec. V. The image of brick accumulations also helps us to recognize the similarity of this model to ballistic aggregation models, whose scaling properties have been studied analytically and numerically [46,47].

Using Eqs. (4) and (5) we obtain the amplitude of the Lyapunov vector of the lth particle as

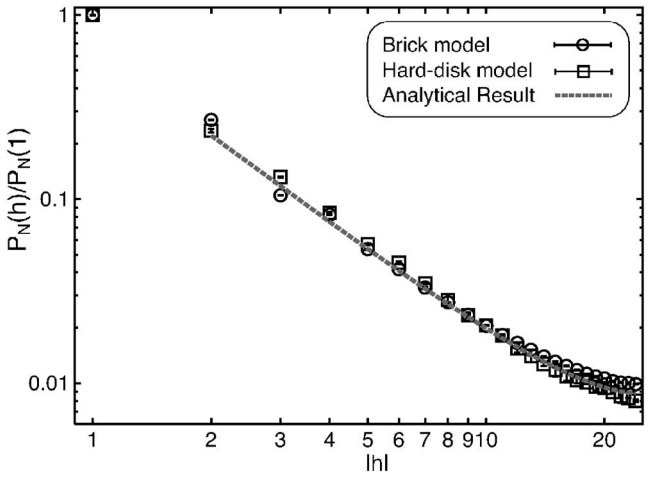

FIG. 5. Log-log plot of the normalized hopping rates $P_N(h)/P_N(1)$ for the brick model (circles) and the quasi-one-dimensional system with $d=10^5$ (squares) as a function of the hopping distance $|h|$ for $N=50$. The error bars are given by $|P_N(h)-P_N(-h)|/P_N(1)$. The broken line is the analytical expression for the hopping rate discussed in Sec. V.

$$|\delta\mathbf{\Gamma}_l(\tau n_t)| \sim |\delta\mathbf{\Gamma}_l(0)|\exp\{-\mathcal{K}_l(n_t)\ln\rho\} \tag{6}$$

after the n_tth particle-particle collisions. From relation (6) between the brick height and the Lyapunov vector, the amplitude of the localized Lyapunov vector components with the highest brick height have much larger values than the other components because of the huge factor $-\ln\rho$ appearing in the exponent of Eq. (6) when $\rho \ll 1$. Therefore, to a good approximation, the normalized amplitude $\gamma_j^{(n)}$ given by Eq. (1) has nonzero components only for particles corresponding to these largest amplitudes, as shown in Fig. 2. The combination of Eqs. (5) and (6) also explains why the amplitudes of the localized components of the Lyapunov vectors for nearest-neighbor particles take almost the same value, thus the normalized amplitude $\gamma_j^{(n)}$ appears as a flat top in the localized regions in Fig. 2. After all, the localized region of the Lyapunov vector represented in Eq. (6) is given as the site indices whose brick height $\mathcal{K}_j(n_t)$ takes the maximum value after the nth brick is dropped, and such sites with the highest brick height can be calculated using the brick model dynamics (5) only, without referring to the hard-disk dynamics. Thus we can calculate the hopping distance h for the brick accumulation model (see Appendix A) and therefore the hopping rate $P_N(h)$, similarly to the quasi-one-dimensional hard-disk system.

Figure 5 shows the normalized hopping rates $P_N(h)/P_N(1)$ for the brick model with 50 sites (circles) and for a quasi-one-dimensional hard-disk system consisting of 50 hard disks and $d=10^5$ (squares). Agreement between the brick model and the quasi-one-dimensional hard-disk system for the normalized hopping rate $P_N(h)/P_N(1)$ for $|h| \geqslant 1$ is satisfactory. Numerical simulations of quasi-one-dimensional hard-disk systems show that the normalized hopping rate $P_N(h)/P_N(1)$ increases very slightly as the density decreases as shown in Appendix A, so the deviation of $P_N(h)/P_N(1)$ in the tail in the brick model and the hard-disk system in Fig. 5 is a finite density effect.

TABLE II. Particle number (N) dependences of the ratio $P_N(0)/P_N(1)$ of the hopping rates at the hopping distances $h=0$ and 1 in the quasi-one-dimensional hard-disk systems with $d=10^3$ and in the brick accumulation model.

N	Hard-disk model $P_N(0)/P_N(1)$	Brick model $P_N(0)/P_N(1)$
25	13.5	17.1
50	26.8	37.9
75	39.6	58.8
100	52.1	79.7

So far we have discussed the hopping rate $P_N(h)$ for nonzero hopping distances $h \neq 0$. Now we discuss the hopping rate $P_N(0)$ for zero hopping distance $h=0$. Table II shows the ratio $P_N(0)/P_N(1)$ for the hopping rates at $h=0$ and 1 in the quasi-one-dimensional hard-disk system with $d=10^3$ and the brick accumulation model for $N=25$, 50, 75, and 100. As shown in this table, the ratio $P_N(0)/P_N(1)$ depends on the number of particles N, and roughly speaking it is proportional to N. To explain this linear dependence of $P_N(0)/P_N(1)$ with respect to N, we note that in the brick model the hopping distance 1 occurs only when a new brick is dropped at one (and not both) of the sites with the highest brick height, meaning that the hopping rate $P_N(1)$ should be approximately inversely proportional to N. On the other hand, the hopping distance 0 occurs when a new brick is dropped at a site which does not have the highest nor the second highest brick height, or is dropped at both the sites which are currently the site of the highest brick height, therefore the hopping rate $P_N(0)$ should be independent of N. These considerations for $P_N(0)$ and $P_N(1)$ explain why the ratio $P_N(0)/P_N(1)$ is proportional to N. However, we need more detailed considerations to explain the difference between the coefficient κ in the relation $P_N(0)/P_N(1) \approx \kappa N$ between the quasi-one-dimensional hard-disk system and the brick accumulation model.

Before finishing, we discuss one more property of the brick accumulation model, which we will use in the next section. Figure 6 is a graph of the sum $\Sigma_{j=1}^N \mathcal{K}_j(n)$ as a function of n. Note that this sum must increase at a speed of more than 2 per dropped brick because accumulated bricks capture spaces below them which cannot be occupied by further dropped bricks. It is clear from this figure that this sum increases linearly, and a fit of the data to the function $\Sigma_{j=1}^N \mathcal{K}_j(n) = \xi + \omega n$ with fitting parameters ξ and ω leads to the values $\xi \approx 0.00$ and $\omega \approx 3.99$ [50]. (Note that data points in the main graph of Fig. 6 look exactly like this fit because of the large scale. In the inset to Fig. 6 we show the graph of $\Sigma_{j=1}^N \mathcal{K}_j(n)$ as a function of n on a much smaller scale, to show its fluctuating behavior.) Therefore, on average, each dropped brick adds a contribution of 4 to the sum $\Sigma_{j=1}^N \mathcal{K}_j(n)$, meaning that each brick occupies not only its own 2 spaces but also captures 2 empty spaces below it.

Note that from Eq. (6) the brick height $\mathcal{K}_j(n)$ dominates the exponential growth rate of the Lyapunov vector compo-

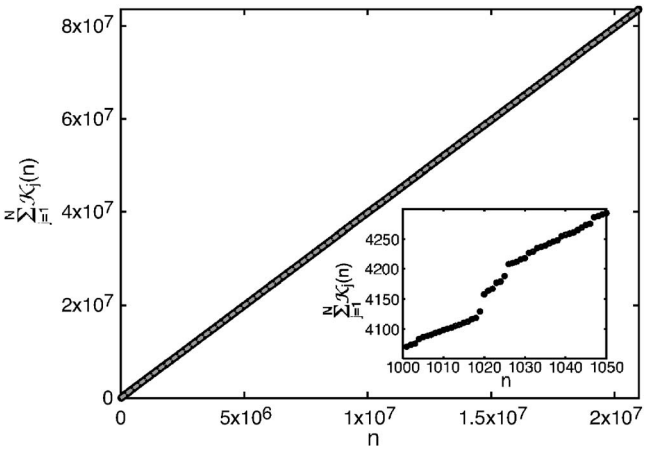

FIG. 6. The sum of the total brick heights as a function of the number n of dropped bricks in the brick model with $N=50$ in the n interval [0, 20979999]. Inset: The same graph but enlarged in the n interval [1000, 1050]. The broken line (which is almost on the data points of the main graph) is a fit of numerical data to a linear function.

nent amplitude. Using this feature of the brick heights, their sum $\Sigma_{j=1}^{N}\mathcal{K}_j(n)$ is connected to the largest Lyapunov exponent $\lambda^{(1)}$ as

$$\lambda^{(1)} \sim -\lim_{n\to+\infty}\frac{1}{n\tau}\left[\frac{1}{N}\sum_{j=1}^{N}\mathcal{K}_j(n)\right]\ln\rho, \tag{7}$$

where the mean free time is τ and the density is ρ in the limit of low density. [See Appendix B for more details on Eq. (7).] As a numerical check of the formula (7) we show in Fig. 7 a graph of the largest Lyapunov exponent $\lambda^{(1)}$ as a function of the density ρ for a quasi-one-dimensional hard-disk system and the brick accumulation model using the formula (7) with

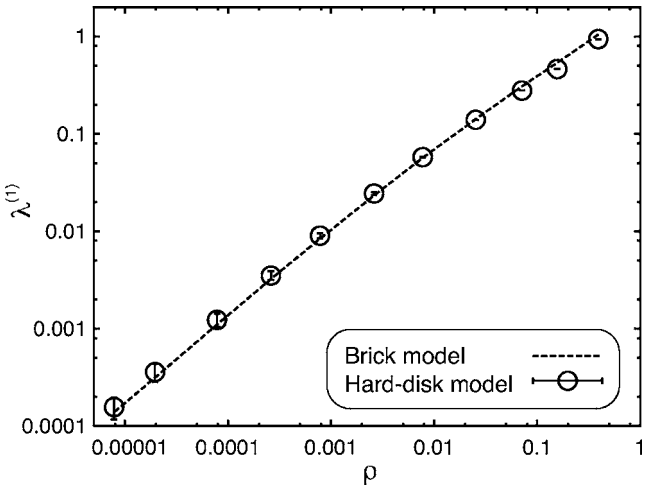

FIG. 7. The largest Lyapunov exponent $\lambda^{(1)}$ as a function of density ρ in a quasi-one-dimensional hard-disk system with $N=50$ as a log-log plot. The error bars are given by $|\lambda^{(1)}-\lambda^{(4N)}|$ which must be zero by the conjugate pairing rule for Hamiltonian systems. The broken line is the largest Lyapunov exponent given by the brick accumulation model with $N=50$.

$N=50$. To calculate the largest Lyapunov exponent from Eq. (7) we used the relation $\Sigma_{j=1}^{N}\mathcal{K}_j(n)\approx 4n$ as shown in Fig. 6 and the values of τ and ρ for the quasi-one-dimensional system whose Lyapunov exponents are plotted in Fig. 7, and the data points are connected by a dashed line for ease of visibility. Figure 7 shows that Eq. (7) reproduces successfully the values of the largest Lyapunov exponent for the quasi-one-dimensional hard-disk systems, not only in the limit of low density but also at relatively high density up to $\rho<0.3$. Note that a linear dependence of the sum $\Sigma_{j=1}^{N}\mathcal{K}_j(n)$ of brick heights with n is necessary to get a finite value of the largest Lyapunov exponent $\lambda^{(1)}$ from Eq. (7).

V. ANALYTICAL EXPRESSION FOR THE HOPPING RATE

In this section we discuss another approach. This is inspired by some of the characteristics of the brick accumulation model discussed in Sec. IV, although we greatly simplified the brick model by omitting some other aspects. The advantage of this approach is that we can get an analytical expression for the hopping rate, while to a good approximation it still reproduces the hopping rate for hard-disk systems. Another important point in this approach is that it connects the dynamics of the localized region of the Lyapunov vectors with a static property, the probability distribution of brick-height differences between nearest-neighbor sites.

In the brick accumulation model, a hop of the highest brick site occurs when two (non-nearest-neighbor) sites have the same brick height. Noting this characteristic we consider the probability distribution $\tilde{P}_\infty(h)$ under the constraint that the two sites μ and $\mu+h$ have the highest brick height. We require that there is no other highest site between the two highest sites μ and $\mu+h$ for $|h|\geq 2$;

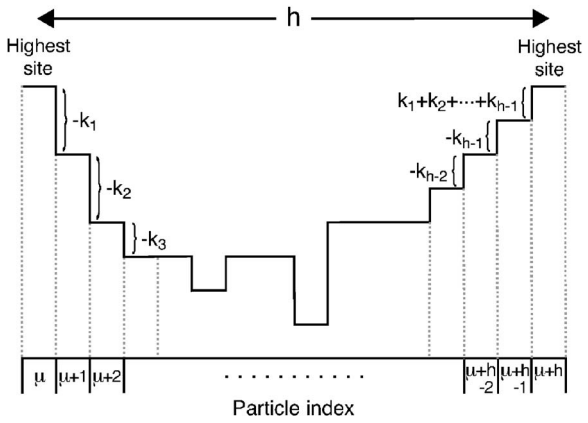

FIG. 8. Schematic illustration for a brick-height configuration (similar to Fig. 4 for the brick model) connecting two highest sites (particle indices) μ and $\mu+h$ with hopping distance h where $h\geq 2$. Here, $-k_l$ is the brick-height difference of the sites $\mu+l-1$ and $\mu+l$. The probability distribution for the configuration of brick-height differences $\{k_l\}\equiv(k_1,\ldots,k_{h-1})$, is given by $\Lambda(-k_1)\Lambda(-k_2)\cdots\Lambda(-k_{h-1})\Lambda(\Sigma_{j=1}^{h-1}k_j)$ with the distribution $\Lambda(k)$ of brick-height differences k between nearest-neighbor sites. The hopping rate $\tilde{P}_\infty(h)$ is calculated as the sum of this probability distribution over possible configurations of brick-heights $\{k_l\}$.

$$\mathcal{K}_l(n) < \mathcal{K}_\mu(n) \quad [=\mathcal{K}_{\mu+h}(n)],$$

in

$$l = \begin{cases} \mu+1, \mu+2, \ldots, \mu+h-1 & \text{for } h \geqslant 2 \\ \mu+h+1, \mu+h+3, \ldots, \mu-1 & \text{for } h \leqslant -2. \end{cases} \tag{8}$$

Using this probability distribution $\tilde{P}_\infty(h)$, we can estimate the hopping rate $P_\infty(h)$ in the thermodynamic limit as the one proportional to $\tilde{P}_\infty(h)$: $P_\infty(h) \propto \tilde{P}_\infty(h)$. Then we can calculate the hopping rate $P_N(h)$ for a finite size system using Eq. (2), apart from a constant factor.

To calculate the probability distribution $\tilde{P}_\infty(h)$ we introduce the distribution $\Lambda(k)$ of brick-height differences k between nearest-neighbor sites. These two distribution functions are connected by

$$\tilde{P}_\infty(h) = \sum_{\substack{k_1 \\ (k_1 \geqslant 1)}} \sum_{\substack{k_2 \\ (k_1+k_2 \geqslant 1)}} \cdots \sum_{\substack{k_{|h|-1} \\ (\sum_{j=1}^{|h|-1} k_j \geqslant 1)}} \times \Lambda(-k_1)\Lambda(-k_2)\cdots\Lambda(-k_{|h|-1})\Lambda \times \left(\sum_{j=1}^{|h|-1} k_j \right). \tag{9}$$

In Eq. (9), $-k_l$ is a brick-height difference of nearest-neighbor sites. The probability distribution for the specific brick-height configuration $\{k_l\}$ is given by $\Lambda(-k_1)\Lambda(-k_2)\cdots\Lambda(-k_{|h|-1})\Lambda(\Sigma_{j=1}^{|h|-1} k_j)$, and the hopping rate $\tilde{P}_\infty(h)$ is calculated as the sum of this probability distribution over all possible configurations of $\{k_l\}$, leading to Eq. (9). Figure 8 is a schematic illustration of a brick-height configuration $\{-k_j\}$ connecting two highest sites for $h \geqslant 2$. In Eq. (9), the lower bounds of the sums on the right-hand side of Eq. (9) come from condition (8). Note that from Eq. (9) the distribution $\tilde{P}_\infty(h)$ is an even function of h, so $\tilde{P}_\infty(-h) = \tilde{P}_\infty(h)$.

Now, for simplicity, we assume that the distribution function $\Lambda(k)$ can be expressed as an exponential function

$$\Lambda(k) = \mathcal{W} \exp\{-\eta|k|\} \tag{10}$$

with constants $\mathcal{W}$ and η (>0). (We will discuss the validity of this assumption later.) Inserting Eq. (10) into Eq. (9), and replacing the sums over k_1 in Eq. (9) with the ones over $k_1' \equiv k_1 + 1$, we obtain

$$\tilde{P}_\infty(h) = \begin{cases} \mathcal{W}^2 \Upsilon \sum_{k=0}^{+\infty} \Upsilon^k & \text{for } |h| = 2, \\ \mathcal{W}^{|h|} \Upsilon \sum_{k_1=0}^{+\infty} \Upsilon^{k_1} \sum_{k_2=-k_1}^{+\infty} \Upsilon^{k_2 \theta(k_2)} \sum_{k_3=-k_1-k_2}^{+\infty} \Upsilon^{k_3 \theta(k_3)} \cdots \sum_{k_{|h|-1}=-\sum_{j=1}^{|h|-2} k_j}^{+\infty} \Upsilon^{k_{|h|-1}\theta(k_{|h|-1})} & \text{for } |h| \geqslant 3, \end{cases} \tag{11}$$

where Υ is defined by

$$\Upsilon \equiv \exp\{-2\eta\} \tag{12}$$

and $\theta(x)$ is the Heaviside function taking the value 1 for $x > 0$ and the value 0 for $x \leqslant 0$. The summations appearing in Eq. (11) can be carried out successively, and we obtain

$$\tilde{P}_\infty(h) = \frac{\mathcal{W}^{|h|}\Upsilon}{(1-\Upsilon)^{|h|-1}} \Omega(|h|), \tag{13}$$

where the function $\Omega(k)$ can be written as

$$\Omega(2) = 1, \tag{14}$$

$$\Omega(3) = 1 + \Upsilon, \tag{15}$$

$$\Omega(4) = 1 + 3\Upsilon + \Upsilon^2, \tag{16}$$

$$\Omega(5) = (1+\Upsilon)(1+5\Upsilon+\Upsilon^2), \tag{17}$$

$$\Omega(6) = 1 + 10\Upsilon + 20\Upsilon^2 + 10\Upsilon^3 + \Upsilon^4, \tag{18}$$

$$\Omega(7) = (1+\Upsilon)(1+14\Upsilon+36\Upsilon^2+14\Upsilon^3+\Upsilon^4), \tag{19}$$

and so on. Equation (13), with Eqs. (14)–(19), etc., gives an analytical expression for the hopping rate, for example, using the relation $P_\infty(h) \propto \tilde{P}_\infty(h)$.

The coefficients $\mathcal{W}$ and η appearing in Eq. (10) can be determined from the two sum rules:

$$\sum_{k=-\infty}^{+\infty} \Lambda(k) = 1, \tag{20}$$

$$\sum_{k=-\infty}^{+\infty} |k| \Lambda(k) = \Delta\mathcal{K}, \tag{21}$$

where $\Delta\mathcal{K}$ is the mean value of the absolute value of the brick height difference between nearest-neighbor sites. The first condition (20) is the normalization of the probability distribution $\Lambda(k)$ which leads to

$$\mathcal{W} = \frac{\exp\{\eta\} - 1}{\exp\{\eta\} + 1}. \tag{22}$$

Using Eq. (22) the second condition (21) gives

$$\eta = \ln\left\{ \frac{1 + \sqrt{1 + \Delta\mathcal{K}^2}}{\Delta\mathcal{K}} \right\}, \tag{23}$$

satisfying the inequality $\eta > 0$. Inserting Eq. (23) into Eqs. (12) and (22) we obtain

$$\Upsilon = \left(\frac{\Delta\mathcal{K}}{1 + \sqrt{1 + \Delta\mathcal{K}^2}} \right)^2 \tag{24}$$

$$\mathcal{W} = \frac{1 + \sqrt{1 + \Delta\mathcal{K}^2} - \Delta\mathcal{K}}{1 + \sqrt{1 + \Delta\mathcal{K}^2} + \Delta\mathcal{K}}. \tag{25}$$

From Eqs. (24) and (25), there is only one parameter $\Delta\mathcal{K}$ remaining to determine the hopping rate using Eq. (13).

To estimate the value of $\Delta\mathcal{K}$, we use a property of the brick accumulation model discussed at the end of Sec. IV. There we showed that $\Sigma_{j=1}^{N} \mathcal{K}_j(n) \approx 4n$. This implies that the averaged brick-height difference between nearest-neighbor sites is about 2, so that

$$\Delta\mathcal{K} \approx 2. \tag{26}$$

We use this value to calculate the hopping rate based on Eq. (13). Notice that from the relation $\Sigma_{j=1}^{N} \mathcal{K}_j(n) \approx (\Delta\mathcal{K} + 2)n$ and the formula (7) we obtain

$$\Delta\mathcal{K} \sim \frac{N\tau}{\ln \rho} \lambda^{(1)} - 2 \tag{27}$$

in the limit of low density. From the relation (27) between the parameter $\Delta\mathcal{K}$ specifying the hopping rate and the largest Lyapunov exponent $\lambda^{(1)}$, the hopping rate of the localized region of the Lyapunov vectors is connected to the largest Lyapunov exponent.

Before comparing the hopping rate based on the analytical expression (13) with the ones for hard-disk systems and the brick accumulation model, we note that this analytical expression for the hopping rate may not be appropriate for small hopping distances $|h|$. In particular, it does not give the correct value of $P_N(1)$ because in the brick model the hopping distance $h = \pm 1$ does not appear from separated highest sites with the same brick height, the assumption used to derive Eq. (13). Therefore it is not appropriate to calculate the hopping rate normalized by $P_N(1)$ from this analytical expression and to compare it with the numerical results. The hopping rate $P_N(\pm 2)$ from Eq. (13) may also be problematic, because in the brick model the hopping distance $h = \pm 2$ occurs when four consecutive sites have the highest brick height, while to derive Eq. (13) we assumed that $h = \pm 2$ occurs when nonconsecutive separate sites μ and $\mu + h$ have the same highest brick height. Based on these considerations we do not calculate the value $P_N(\pm 1)$ from the analytical approach in this section, and plot the hopping rate so that $P_N(5)$ by Eq. (13) gives the same value as that from the brick model.

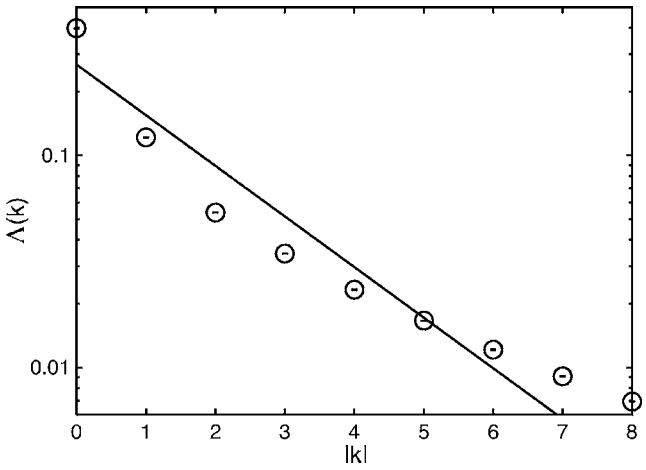

FIG. 9. A log-linear plot of the distribution $\Lambda(k)$ of brick-height differences k between nearest-neighbor sites as a function of $|k|$ in the brick accumulation model with $N = 50$. Here, $\Lambda(k)$ is normalized by $\Sigma_{k=-2N}^{2N} \Lambda(k) = 1$. The distribution $\Lambda(k)$ is an even function of k, and the error bars in this graph are given by $|\Lambda(k) - \Lambda(-k)|$. The line is an exponential function used to obtain the analytical expression for the hopping rate given by Eqs. (10) and (24)–(26).

In Fig. 5 for the normalized hopping rate $P_N(h)/P_N(1)$ we plotted the function $\Psi(h) \equiv \widetilde{P}_N(h) P_N(5) / [\widetilde{P}_N(5) P_N(1)]$ using the value $P_N(5)/P_N(1)$ of the brick model with $\widetilde{P}_N(h) = \widetilde{P}_\infty(h) + \widetilde{P}_\infty(N - h)$ using the analytical expression $\widetilde{P}_\infty(h)$ given by Eq. (13) for $|h| \geqslant 2$. Note $\Psi(5) = P_N(5)/P_N(1)$ so that $\Psi(h)$ coincides with $P_N(h)/P_N(1)$ of the brick model at $|h| = 5$. Here, the values of the hopping rate are given at integer values of h, but we connect them with a broken line for ease of visibility. Figure 5 shows that the analytical expression (13) for the hopping rate reproduces the hopping rate for the brick accumulation model as well as the quasi-one-dimensional hard-disk system to a good approximation. It may be noted that for this plot we used the first two dominant terms on the right-hand side of Eq. (2), and part of the small deviation of the hopping rate in the tail between the brick model and the analytical expression should come from the omission of higher order terms in Eq. (2).

We notice that the approach in this section is simple enough to get an analytical expression for the hopping rate but it is not completely consistent with the brick accumulation model discussed in Sec. IV. Previously, we have mentioned the irrelevance of Eq. (13) as a description of a small hopping rate in the brick model. Actually, in the approach of this section we omitted the essential characteristic of the bricks as components of the brick accumulation model, except for the property (26), and treated the model components as blocks (or half bricks). As another example, we show in Fig. 9 the numerical result for the distribution $\Lambda(k)$ of brick-height differences k between nearest-neighbor sites in the brick accumulation model with $N = 50$. Here, $\Lambda(k)$ is normalized by $\Sigma_{k=-2N}^{2N} \Lambda(k) = 1$, instead of Eq. (20), because we cannot calculate $\Lambda(k)$ in $|k| \to +\infty$ numerically. In this figure we added the exponential distribution (10) using Eqs. (24)–(26). Figure 9 shows that the probability distribution $\Lambda(k)$ does not coincide with an exponential distribution (10), although it

may be justified as a first approximation. [On the other hand, the numerical evaluation of $\Delta\mathcal{K}$ from the distribution $\Lambda(k)$ as a numerical result in Fig. 9 gives the value 1.99, then Eq. (26) is still justified.] On another point, in the brick model the highest brick sites appear as a pair of nearest-neighbor sites, but we did not take into account this characteristic in the analytical approach in this section. Despite the omission of characteristics of the brick accumulation model, the analytical approach in this section reproduces the hopping rate for many-hard-disk systems reasonably well, and it suggests that this approach still keeps enough of the essential characteristics that describe the dynamics of the Lyapunov localization.

VI. CONCLUSION AND REMARKS

We have discussed the dynamics of the spatially localized region of the Lyapunov vector corresponding to the largest Lyapunov exponent for a quasi-one-dimensional hard-disk system. The dynamics of the localized region of the Lyapunov vector is described by a hopping rate, and the hopping rate decreases as the absolute value of hopping distance increases. We can explain this quantitatively in two ways: a brick accumulation model; and an analytical approach. In the brick accumulation model, the hopping behavior of the localized Lyapunov vectors was explained as a change of the highest brick position. It was shown that using this brick model we can calculate the largest Lyapunov exponent for quasi-one-dimensional hard-disk systems. On the other hand, in the analytical approach the hopping rate was calculated from probability distributions for brick height differences between nearest-neighbor sites, via multiple summations over all possible configurations that connect two separated highest sites. The result is related to the largest Lyapunov exponent. Both of the approaches successfully reproduced the hopping-distance dependence of the hopping rate for the localized Lyapunov vectors of quasi-one-dimensional hard-disk systems.

Before we began this work, there had been a view that the origin of the hopping behavior of localized Lyapunov vectors was

⟨*Conjecture*⟩ *The localized region of the Lyapunov vector hops to the position of a new grazing collision.*

This conjecture was suggested from the fact that a change of Lyapunov vectors in particle collisions may be dominated by the factor $1/(\boldsymbol{\sigma}\cdot\Delta\boldsymbol{p})$ in the collision dynamics (see Appendix B), where $\boldsymbol{\sigma}$ is the normalized collision vector and $\Delta\boldsymbol{p}$ is the momentum difference of the colliding particles before the collision. This argument suggests that if two particles collide at a small angle (a grazing collision, where $|\boldsymbol{\sigma}\cdot\Delta\boldsymbol{p}|$ is small), then the Lyapunov vector can change significantly and the position of the localized region may move. However, this scenario cannot be correct for the following reasons.

(1) This conjecture implies that as the position at which a grazing collision occurs is random, the hopping distance should also be random. This contradicts our numerical result that the hopping rate decreases with increasing the absolute value of hopping distance, as shown in Fig. 3.

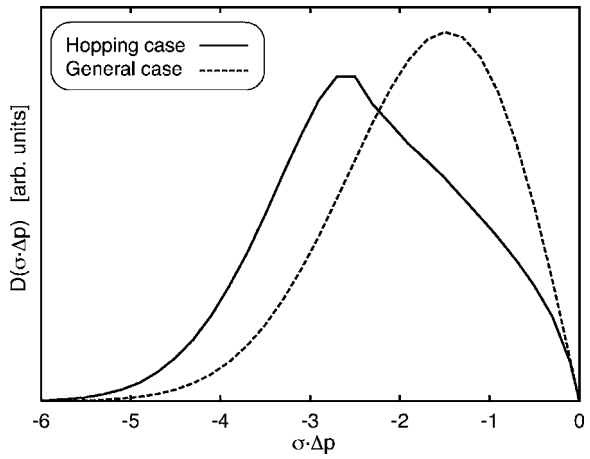

FIG. 10. The distribution $D(\boldsymbol{\sigma}\cdot\Delta\boldsymbol{p})$ of the quantity $\boldsymbol{\sigma}\cdot\Delta\boldsymbol{p}$ with the normalized collision vector $\boldsymbol{\sigma}$ and the momentum difference $\Delta\boldsymbol{p}$ of colliding particles just before the collision; for the general case (dashed line) and for the case (solid line) in which nonzero hopping of a localized Lyapunov vector occurs. The system is a quasi-one-dimensional system with $d=10^3$ and $N=25$.

(2) We show in Fig. 10 the distribution $D(\boldsymbol{\sigma}\cdot\Delta\boldsymbol{p})$ of $\boldsymbol{\sigma}\cdot\Delta\boldsymbol{p}$ in general collisions (dashed line) and the distribution in collisions causing hopping of the localized Lyapunov vector (solid line) [51]. It is clear from Fig. 10 that the quantity $|\boldsymbol{\sigma}\cdot\Delta\boldsymbol{p}|$ is not smaller in collisions which lead to jumps of the localized region of the Lyapunov vector.

We note that the hopping dynamics of the Lyapunov vector for the brick accumulation model described in Sec. IV is independent of collision parameters. This also suggests that the above conjecture for the origin of the hopping of the localized region of the Lyapunov vector cannot be justified. On the other hand, this collision parameter independence of the hopping behavior in the brick model cannot explain why the distribution $D(\boldsymbol{\sigma}\cdot\Delta\boldsymbol{p})$ for the hopping case is different from the general case. This remains an open problem.

The fits of the hopping rate with distance in Fig. 3 suggest a power law: $\boldsymbol{P}_\infty(h)\sim|h|^{-\beta}$ with $\beta\approx 1.7$. The value of β decreases weakly with decreasing density as shown in Table III and this appears to be consistent with the brick model where $\beta\approx 1.5$ for $N=1000$. It is plausible that the value of β from the brick accumulation model may represent the low density limit.

The hopping rate of the localized region of a Lyapunov vector, and the largest Lyapunov exponent, are well described by the brick accumulation model. One may ask for a

TABLE III. Fitting parameters for the function $f(h)$ shown in Fig. 13 for quasi-one-dimensional systems of different system lengths with $N=50$. The system length L_x is related to the parameter d as $L_x=NL_y(1+d)$. Notice that the coefficient β decreases slightly as the system length increases.

d	α	β
10^3	0.79±0.02	1.72±0.01
10^4	0.80±0.02	1.69±0.01
10^5	0.82±0.02	1.69±0.01

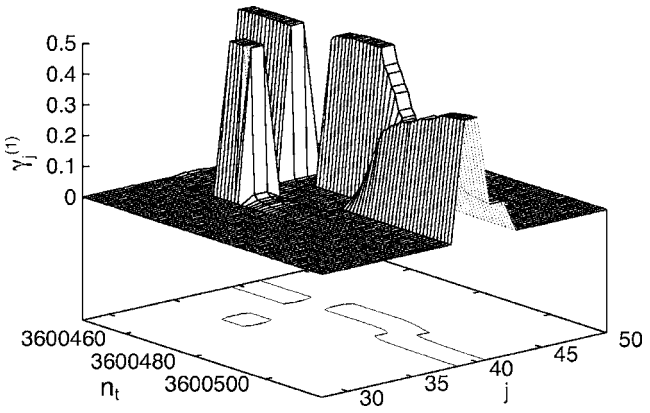

FIG. 11. The normalized amplitude $\gamma_j^{(1)}$ of the Lyapunov vector component $\delta\mathbf{\Gamma}_j^{(1)}$ corresponding to the largest Lyapunov exponent $\lambda^{(1)}$ as a function of the collision number n_t and the particle index j in a quasi-one-dimensional system with $d=10^4$ and $N=50$. Here, the collision number interval shown in this graph is $[k,k+68]$ with $k=3\,600\,448$. On the base of this graph is a contour plot of $\gamma_j^{(1)}$ at the level 0.2. Three hops of the localized region of the Lyapunov vector are visible in this time interval; the first two hops are sharp and the last one is gradual.

more direct numerical check of the justification of the brick accumulation model in quasi-one-dimensional hard-disk systems, by, for example, checking Eq. (6) or observing numerically an actual brick configuration such as that presented in Fig. 4. However, such a check of the brick model is not trivial for the following reasons. First, the brick accumulation model is only justified in the limit of low density, but numerical simulations have to be at some finite density. This effect appears, for example, as gradual changes of the Lyapunov vector component amplitudes, as shown in Fig. 11, which do not appear in the brick accumulation model. Second, even if we could simulate at an extremely low density in which such finite density effects can be neglected (although the case presented in this paper is not at such a low density), the factor $-\ln\rho$ in Eq. (6) may be too large for an actual numerical calculation.

In order to introduce the hopping rate we used the property of quasi-one-dimensional systems, that the order of particles is an invariant. In this sense, it is not straightforward to generalize our argument to fully two- (or three-) dimensional systems. An effective way to describe the dynamics for the localized region of the Lyapunov vectors for higher spatial dimensions remains an important future problem. It should be noted that it is known that the clock model version of the brick accumulation model itself can be easily generalized to any spatial dimensional case, although in higher dimension we do not have the concept of the accumulation of bricks, as we did for the quasi-one-dimensional case.

Finally, the brick accumulation model (more generally the clock model) used in this paper has been justified for hard-disk (or hard-sphere) systems only (at least so far). However, Lyapunov localization is observed not only in many-hard-disk systems but also in a wide variety of other systems with many degrees of freedom, such as the Kuramoto-Sivashinsky model [22], a random matrix model [24], map systems [23,25,48,49], and coupled nonlinear oscillators [27], etc. It is a challenge to develop approaches to the dynamics of Lyapunov localization for this wider class of systems.

ACKNOWLEDGMENTS

One of the authors (T.T.) wishes to thank R. van Zon, who indicated the possibility of describing the hopping dynamics for the localized Lyapunov vectors using the clock model and supplied a computer program for the clock model. We also appreciate helpful discussions with E. Zabey and J.-P. Eckmann. In particular, they suggested the importance of the difference of brick heights for nearest-neighbor sites in the calculation of the hopping rate, and posed a question about the behavior of the sum of brick heights as shown in Fig. 6, and also indicated the analogy between the brick accumulation model and ballistic aggregation models. We also thank H. A. Posch for a comment on Lyapunov localization, which sparked our interest in this problem. The authors appreciate the financial support of the Japan Society for the Promotion of Science.

APPENDIX A: HOPPING RATE OF A LOCALIZED LYAPUNOV VECTOR

In this appendix we give the detailed definition of the hopping rate for the localized region of the Lyapunov vectors, which is used in this paper. As suggested in Refs. [29,38], the normalized Lyapunov vectors corresponding to the largest Lyapunov exponent have large components for only two particles in the low density limit, and changes of these large components are caused by particle collisions. Applying this characteristic of the Lyapunov vector to the quasi-one-dimensional system with periodic boundary conditions, we can introduce a hopping distance $h^{[n]}$ at the nth collision as

$$h^{[n]} = j_{n+1} - j_n - N\,\mathrm{nint}\left\{\frac{j_{n+1}-j_n}{N}\right\}. \tag{A1}$$

Here $\{j_n, j_n+1\}$ are the large components before the nth collision and $\{j_{n+1}, j_{n+1}+1\}$ are the large components just after the nth collision. The function $\mathrm{nint}\{x\}$ is the closest integer to the real number x. We assume that changes in the position of the localized region of the Lyapunov vector are negligible during the free-flight interval, so $\{j_{n+1}, j_{n+1}+1\}$ can also be interpreted as the set of the particle indices whose Lyapunov vector components take large values just before the $(n+1)$th collision. We count the number of times $\mathcal{N}_T(h)$ that we see a hop of size h in a time-interval T where $-[N/2] \leqslant h \leqslant [N/2]$. The normalized hopping rate $p_N(h)$ can be introduced as $P_N(h)/P_N(1) = \lim_{T\to\infty} \mathcal{N}_T(h)/\mathcal{N}_T(1)$.

However, in actual numerical simulations, the particle density ρ is always finite, and large Lyapunov components of more than two particles can often be seen, at least down to a density $\rho \approx 10^{-5}$ which is the low density limit of the numerical simulations in this paper. This makes the above definition (A1) of the hopping distance $h^{[n]}$ impractical. To explain this point concretely we show Fig. 11, which is a graph of the normalized Lyapunov vector component amplitude $\gamma_j^{(1)}$ de-

fined by Eq. (1) as a function of the collision number n_t and the particle index j in a quasi-one-dimensional system with $N=50$ and $d=10^4$ (namely a density $\rho \approx 7.85 \times 10^{-5}$). In this figure we can recognize three types of hops of the localized region of the Lyapunov vector. The first two hops keep the large Lyapunov vector components of almost two particles sharp enough to apply the definition (A1) of the hopping distance, but the third hop occurs gradually so that no clear hopping time can be determined. Note that the localized region of Lyapunov vector component amplitudes in the three-dimensional plot 11 always has a flat top with a width of two-particles even for the third hop in Fig. 11.

For concrete calculations, we define the localized region of the Lyapunov vector components as the particle indices j for which $\gamma_j^{(n)} > 0.2$. (Here, we use the similarity between particle positions and particle indices for the quasi-one-dimensional system.) In Fig. 11, this localized region is approximately given by the region surrounded by the contour lines (level 0.2) on the base of the graph. We introduce the quantity l_n as the number of particles satisfying the inequality $\gamma_j^{(n)} > 0.2$ just before the nth collision. Note that $0 \leqslant \gamma_j^{(n)} \leqslant 1$ by definition (1) of $\gamma_j^{(n)}$, so l_n cannot be equal to nor larger than 5. If l_n is always 2 as in the low density limit, then we can use the hopping distance definition (A1), but in numerical simulations at finite density $l_n > 2$ can happen as shown in Fig. 11. The problem then is how do we define the hopping distance $h^{[n]}$ at the nth collision, when $l_n > 2$.

The definitions of the hopping distance for each case are categorized as follows.

$\langle$*Case (a)*: $l_n=2 \rightarrow l_{n+1}=2\rangle$ Here only two particle indices are in the localized region before and after the collision, and they are always nearest-neighbors, so the hopping distance $h^{[n]}$ is given by Eq. (A1).

$\langle$*Case* $(b1)$: $l_n=2 \rightarrow l_{n+1}=3\rangle$ Here we assume that the localized regions of the Lyapunov vector are given by $\{j_n, j_n+1\}$, $\{j_{n+1}, j_{n+1}+1, j_{n+1}+2\}$, and $j_{n+1}=j_n$ or $j_{n+1}=j_n-1$. We take the value of the hopping distance to be 1 (-1) for $h^{[n]}$ where $j_{n+1}=j_n$ $(j_{n+1}=j_n-1)$.

$\langle$*Case* $(b2)$: $l_n=3 \rightarrow l_{n+1}=2\rangle$ In this case we assume that the localized regions of the Lyapunov vector are given by $\{j_n, j_n+1, j_n+2\}$, $\{j_{n+1}, j_{n+1}+1\}$, and $j_{n+1}=j_n$ or $j_{n+1}=j_n+1$, and the hopping distance is 0 in both cases.

$\langle$*Case* $(b3)$: $l_n=3 \rightarrow l_{n+1}=3\rangle$ In this case we assume that the localized regions of the Lyapunov vector are given by $\{j_n, j_n+1, j_n+2\}$, $\{j_{n+1}, j_{n+1}+1, j_{n+1}+2\}$, and $j_{n+1}=j_n+h^{[n]}$ with the hopping distance $h^{[n]}$. We take into account the case $h^{[n]}=-1, 0$ or 1 only.

$\langle$*Case* $(c1)$: $l_n=2 \rightarrow l_{n+1}=4\rangle$ In this case we assume that the localized regions of the Lyapunov vector are given by $\{j_n, j_n+1\}$, $\{j_{n+1}, j_{n+1}+1\}$, and $\{j'_{n+1}, j'_{n+1}+1\}$ satisfying $j'_{n+1}=j_n$ and $|j'_{n+1}-j_{n+1}| \geqslant 2$. The hopping distance is defined by Eq. (A1) using these j_{n+1} and j_n.

$\langle$*Case* $(c2)$: $l_n=4 \rightarrow l_{n+1}=2\rangle$ In this case we assume that the localized regions of the Lyapunov vector are given by $\{j_n, j_n+1\}$, $\{j'_n, j'_n+1\}$, and $\{j_{n+1}, j_{n+1}+1\}$ satisfying $|j_n-j'_n| \geqslant 2$ and $|j_n-j_{n+1}| \leqslant 1$. The hopping distance $h^{[n]}$ is $h^{[n]}=j_{n+1}-j_n=-1, 0$ or 1.

$\langle$*Case* $(c3)$: $l_n=4 \rightarrow l_{n+1}=4\rangle$ In this case we consider only the case in which the localized regions of Lyapunov vector are given by $\{j_n, j_n+1\}$, $\{j'_n, j'_n+1\}$, $\{j_{n+1}, j_{n+1}+1\}$, and $\{j'_{n+1}, j'_{n+1}+1\}$ satisfying $j_{n+1}=j_n$, $j'_{n+1}=j'_n$, and $|j_n-j'_n| \geqslant 2$. The hopping distance takes the value 0 in this case.

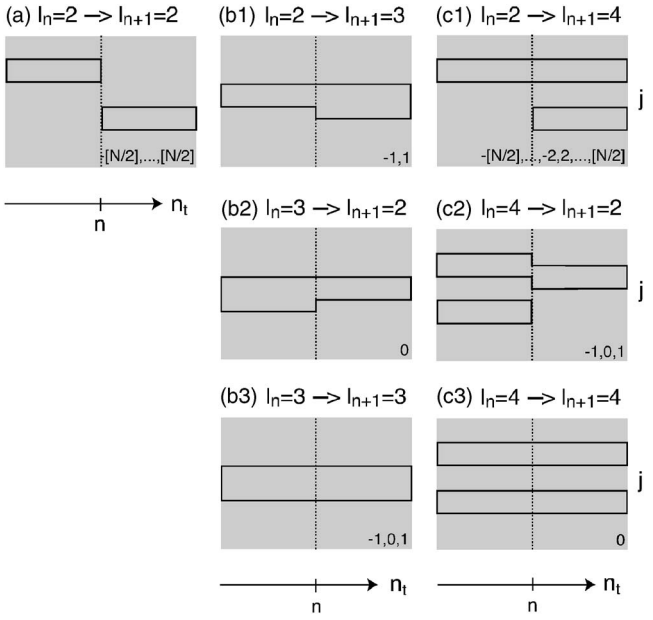

FIG. 12. Schematic illustrations of the hopping types for the localized region of the Lyapunov vector in quasi-one-dimensional systems at low density. The contours represent the level $\gamma_j^{(1)}=0.2$. (These are the contours on the base of Fig. 11.) The vertical dotted line is collision number n at which the hopping distance of the localized Lyapunov vector is to be determined. The seven illustrations in this figure indicate: (a) the case of $(l_n, l_{n+1})=(2,2)$, (b1) the case of $(l_n, l_{n+1})=(2,3)$, (b2) the case of $(l_n, l_{n+1})=(3,2)$, (b3) the case of $(l_n, l_{n+1})=(3,3)$, (c1) the case of $(l_n, l_{n+1})=(2,4)$, (c2) the case of $(l_n, l_{n+1})=(4,2)$, and (c3) the case of $(l_n, l_{n+1})=(4,4)$, where l_n is the number of particles in the localized region of the Lyapunov vector just before the nth collision. The numbers in the right-bottom of each illustration give the possible values of the hopping distance.

(For each case above, the corresponding schematic illustration is shown in Fig. 12.) Here, we use periodic boundary conditions for the particle index, so that the localized regions $\{N, 1\}$, $\{N, 1, 2\}$, and $\{N-1, N, 1\}$ should be translated to $\{0, 1\}$, $\{0, 1, 2\}$, and $\{-1, 0, 1\}$, respectively, in the above definition of the hopping distance. In the examples shown in Fig. 11, the first two hops of the localized Lyapunov vector can be described as case (a), and the third hop is described as cases (c1) and (c2). Note that asymmetric definitions of hopping distances $h^{[n]}$ between cases (c1) and (c2) [and similarly between cases (b1) and (b2)] are required so that we can interpret the hopping distance of the third nonzero hop in Fig. 11 as only -2 in spite of it involving both cases (c1) and (c2). Using the above hopping distance we count the number $\mathcal{N}_T(h)$ of hops of distance h in time interval T, and introduce the normalized hopping rate as $P_N(h)/P_N(1) \equiv \lim_{T \to \infty} \mathcal{N}_T(h)/\mathcal{N}_T(1)$ for $h=-[N/2], -[N/2]+1, \ldots, [N/2]$. Notice that there are possibilities apart from those shown above, but it is observed

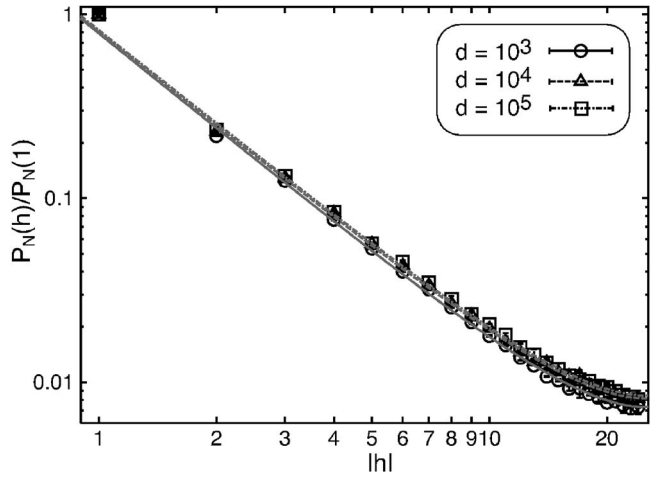

FIG. 13. Log-log plots of the normalized hopping rates $P_N(h)/P_N(1)$ for a quasi-one-dimensional system of 50 hard disks as a function of the hopping distance $|h|$ at different densities, $d=10^3$ (circles), 10^4 (triangles), and 10^5 (squares). The density is a function of d given by $\rho=\pi R^2/[(1+d)L_y^2]$. The error bars are given by $|P_N(h)-P_N(-h)|/P_N(1)$. The lines (solid line for $d=10^3$, broken line for $d=10^4$, and broken line interrupted by dots for $d=10^5$) are fitting the numerical data for $P_N(h)/P_N(1)$ to the function $f(h)\equiv\alpha\Sigma_{j=-2}^{2}|h+jN|^{-\beta}$ assuming that the decay of $P_\infty(h)\propto|h|^{-\beta}$ with fitting parameters α and β, and the values of the fitting parameters α and β are given in Table III.

that in numerical simulations the probabilities of these are extremely small (for example, more than 96% of all hops could be categorized this way).

In Fig. 13 we show the normalized hopping rate $P_N(h)/P_N(1)$ in a quasi-one-dimensional system of 50 hard disks. The hopping rate is almost density-independent in this low density range, although it may be very slightly larger at the lowest density for $|h|=2,3,\ldots$. This slight density dependence of the normalized hopping rate at low density is also expressed as a slight decreasing of the parameter β, as shown in Table III, with density.

We also calculate the hopping rate for the brick accumulation model explained in Sec. IV in a similar way. In the brick accumulation model we can introduce the localized region of the Lyapunov vectors as the site (particle) whose brick height is highest. For the brick model, cases (b1), (b2), and (b3) above cannot happen, and only cases (a), (c1), (c2), and (c3) above are taken into account in the numerical calculations. Note that in the brick model, case (a) above can happen only when the hopping distance is -1, 0, or 1, and Eq. (A1) alone is not enough to calculate the hopping distance. This is another reason to take into account the case where $l_n>2$ in the calculation of the hopping distance.

APPENDIX B: CLOCK MODEL FOR MANY-HARD-PARTICLE SYSTEMS

Here we give an extension of the derivation of the clock model for the Lyapunov vector dynamics in many-hard-particle systems in the limit of low density. We also derive the formula (7) for the largest Lyapunov exponent from the clock model. The one-dimensional version of the clock model is the brick accumulation model used in this paper. In particular, we clarify the assumptions needed to justify the use of this model to discuss the Lyapunov localization. For the basic idea of the clock model, see, for example, Refs. [36,37]. However, note that our notation and assumptions are a little different so that the derived clock model is consistent with the discussions in this paper and able to be compared with the numerical results of Ref. [29].

We consider a $\mathcal{D}$-dimensional system with N hard disks (or hard spheres, etc.) with identical radius R and mass M. We assume that there is no external field so that the dynamics is simply free-flights, and collisions between pairs of particles. The Lyapunov vector components are $(\delta\boldsymbol{q}_l,\delta\boldsymbol{p}_l)^T$ with the transpose T, where $\delta\boldsymbol{q}_l$ is the spatial component of the lth particle, and $\delta\boldsymbol{p}_l$ is the momentum component.

We take t_n to be the time of the nth collision involving particles j and k, and define $\tau_n\equiv(t_n-t_{n-1})/M$, so that the nth free-flight time is given by $\tau_n M$. The free-flight part of dynamics of the Lyapunov vector is represented as

$$\delta\boldsymbol{q}_l(t_n^-)=\delta\boldsymbol{q}_l(t_{n-1}^+)+\tau_n\delta\boldsymbol{p}_l(t_{n-1}^+), \tag{B1}$$

$$\delta\boldsymbol{p}_l(t_n^-)=\delta\boldsymbol{p}_l(t_{n-1}^+). \tag{B2}$$

Here, the superscript $\pm$ refers to the limit of the quantity before the nth collision $(-)$ or after the nth collision $(+)$. The change in the Lyapunov vector in the collision between particles j and k is represented as [45]

$$\delta\boldsymbol{q}_j(t_n^+)=\delta\boldsymbol{q}_j(t_n^-)+\Theta^{[n]}\delta\boldsymbol{q}_{k,j}(t_n^-), \tag{B3}$$

$$\delta\boldsymbol{q}_k(t_n^+)=\delta\boldsymbol{q}_k(t_n^-)-\Theta^{[n]}\delta\boldsymbol{q}_{k,j}(t_n^-), \tag{B4}$$

$$\delta\boldsymbol{p}_j(t_n^+)=\delta\boldsymbol{p}_j(t_n^-)+\Theta^{[n]}\delta\boldsymbol{p}_{k,j}(t_n^-)+\mathcal{Q}^{[n]}\delta\boldsymbol{q}_{k,j}(t_n^-), \tag{B5}$$

$$\delta\boldsymbol{p}_k(t_n^+)=\delta\boldsymbol{p}_k(t_n^-)-\Theta^{[n]}\delta\boldsymbol{p}_{k,j}(t_n^-)-\mathcal{Q}^{[n]}\delta\boldsymbol{q}_{k,j}(t_n^-) \tag{B6}$$

Note that $\delta\boldsymbol{q}_l(t_n^+)=\delta\boldsymbol{q}_l(t_n^-)$ and $\delta\boldsymbol{p}_l(t_n^+)=\delta\boldsymbol{p}_l(t_n^-)$ for $l\notin\{j,k\}$. We have used $\delta\boldsymbol{q}_{k,j}\equiv\delta\boldsymbol{q}_k-\delta\boldsymbol{q}_j$, $\delta\boldsymbol{p}_{k,j}\equiv\delta\boldsymbol{p}_k-\delta\boldsymbol{p}_j$, and $\Theta^{[n]}$ and $\mathcal{Q}^{[n]}$ are defined by

$$\Theta^{[n]}\equiv\boldsymbol{\sigma}^{[n]}\boldsymbol{\sigma}^{[n]T}, \tag{B7}$$

$$\mathcal{Q}^{[n]}\equiv\frac{\boldsymbol{\sigma}^{[n]T}\Delta\boldsymbol{p}^{[n]}}{2R}\left(I+\frac{\boldsymbol{\sigma}^{[n]}\Delta\boldsymbol{p}^{[n]T}}{\boldsymbol{\sigma}^{[n]T}\Delta\boldsymbol{p}^{[n]}}\right)\left(I-\frac{\Delta\boldsymbol{p}^{[n]}\boldsymbol{\sigma}^{[n]T}}{\Delta\boldsymbol{p}^{[n]T}\boldsymbol{\sigma}^{[n]}}\right) \tag{B8}$$

with $\boldsymbol{\sigma}^{[n]}\equiv[\boldsymbol{q}_k(t_n^-)-\boldsymbol{q}_j(t_n^-)]/[|\boldsymbol{q}_k(t_n^-)-\boldsymbol{q}_j(t_n^-)|]$ and $\Delta\boldsymbol{p}^{[n]}\equiv\boldsymbol{p}_k(t_n^-)-\boldsymbol{p}_j(t_n^-)$ and the $\mathcal{D}\times\mathcal{D}$ identity matrix I. Note that all vectors in this appendix are column vectors, so, for example, $\boldsymbol{\sigma}^{[n]T}\Delta\boldsymbol{p}^{[n]}$ is a scalar and $\boldsymbol{\sigma}^{[n]}\Delta\boldsymbol{p}^{[n]T}$ is a matrix. For later use we note that

$$\delta\boldsymbol{p}_j(t_n^+)+\delta\boldsymbol{p}_k(t_n^+)=\delta\boldsymbol{p}_j(t_n^-)+\delta\boldsymbol{p}_k(t_n^-) \tag{B9}$$

which can be derived from Eqs. (B5) and (B6).

We consider the low density case, in which the free-flight time $\tau_n M$ is large (so $\tau_n \propto 1/\rho$). This justifies our first approximation for the Lyapunov vector:

$$\delta \boldsymbol{q}_l(t_n^-) \sim \tau_n \delta \boldsymbol{p}_l(t_{n-1}^+) \tag{B10}$$

where the term containing τ_n is much larger than the other term on the right-hand side of Eq. (B1). This asymptotic relation (B10) leads to

$$\delta \boldsymbol{q}_{k,j}(t_n^-) \sim \tau_n \delta \boldsymbol{p}_{k,j}(t_{n-1}^+) \tag{B11}$$

from the definition of $\delta \boldsymbol{q}_{k,j}(t_n^-)$ and $\delta \boldsymbol{p}_{k,j}(t_{n-1}^+)$. Using the relation (B11), Eqs. (B5) and (B6) can be rewritten as

$$\delta \boldsymbol{p}_j(t_n^+) \sim \delta \boldsymbol{p}_j(t_{n-1}^+) + \Theta^{[n]} \delta \boldsymbol{p}_{k,j}(t_{n-1}^+) + \tau_n \mathcal{Q}^{[n]} \delta \boldsymbol{p}_{k,j}(t_{n-1}^+), \tag{B12}$$

$$\delta \boldsymbol{p}_k(t_n^+) \sim \delta \boldsymbol{p}_k(t_{n-1}^+) - \Theta^{[n]} \delta \boldsymbol{p}_{k,j}(t_{n-1}^+) - \tau_n \mathcal{Q}^{[n]} \delta \boldsymbol{p}_{k,j}(t_{n-1}^+), \tag{B13}$$

where we have used Eq. (B2) to make all the time arguments on the right-hand side (rhs) the same. Note that the spatial part of the Lyapunov vector does not appear in these dynamics and the first and second terms on the rhs of Eqs. (B12) and (B13) are negligible compared with the third term because τ_n is very large, so we obtain

$$\delta \boldsymbol{p}_j(t_n^+) \sim \tau_n \mathcal{Q}^{[n]} \delta \boldsymbol{p}_{k,j}(t_{n-1}^+), \tag{B14}$$

$$\delta \boldsymbol{p}_k(t_n^+) \sim -\tau_n \mathcal{Q}^{[n]} \delta \boldsymbol{p}_{k,j}(t_{n-1}^+), \tag{B15}$$

which lead to

$$\delta \boldsymbol{p}_j(t_n^+) + \delta \boldsymbol{p}_k(t_n^+) \sim 0. \tag{B16}$$

On the other hand, for the dynamics given by Eqs. (B3) and (B4) for the spatial part of the Lyapunov vector we obtain

$$\delta \boldsymbol{q}_j(t_n^+) \sim \tau_n [\delta \boldsymbol{p}_j(t_{n-1}^+) + \Theta^{[n]} \delta \boldsymbol{p}_{k,j}(t_{n-1}^+)], \tag{B17}$$

$$\delta \boldsymbol{q}_k(t_n^+) \sim \tau_n [\delta \boldsymbol{p}_k(t_{n-1}^+) - \Theta^{[n]} \delta \boldsymbol{p}_{k,j}(t_{n-1}^+)], \tag{B18}$$

using Eqs. (B10) and (B11). Now we note

$$\delta \boldsymbol{p}_j(t_{n-1}^+) = \frac{\delta \boldsymbol{p}_j(t_n^+) + \delta \boldsymbol{p}_k(t_n^+)}{2} - \frac{\delta \boldsymbol{p}_{k,j}(t_{n-1}^+)}{2} \sim -\frac{\delta \boldsymbol{p}_{k,j}(t_{n-1}^+)}{2} \tag{B19}$$

where we used Eqs. (B2), (B9), and (B16). Similarly we have

$$\delta \boldsymbol{p}_k(t_{n-1}^+) \sim \frac{\delta \boldsymbol{p}_{k,j}(t_{n-1}^+)}{2}. \tag{B20}$$

Therefore Eqs. (B17) and (B18) can be rewritten as

$$\delta \boldsymbol{q}_j(t_n^+) \sim \tau_n \mathcal{R}^{[n]} \delta \boldsymbol{p}_{k,j}(t_{n-1}^+), \tag{B21}$$

$$\delta \boldsymbol{q}_k(t_n^+) \sim -\tau_n \mathcal{R}^{[n]} \delta \boldsymbol{p}_{k,j}(t_{n-1}^+), \tag{B22}$$

where $\mathcal{R}^{[n]}$ is defined by $\mathcal{R}^{[n]} \equiv -(1/2)I + \Theta^{[n]}$. The asymptotic equations (B14), (B15), (B21), and (B22), give the Lyapunov vector dynamics in the limit of low density. It should also be noted that the assumptions used to derive this dynamics breaks some conservation laws in the original dynamics, for example, the quantity $\Sigma_{l=1}^N \delta \boldsymbol{p}_l(t)$ is conserved in the original dynamics (B2), (B5), and (B6) but this cannot be guaranteed exactly in the low density dynamics (B14) and (B15).

Now we consider the Lyapunov vector $\delta\boldsymbol{\Gamma}$ corresponding to a positive Lyapunov exponent. The positivity of the Lyapunov exponent means that the amplitude $|\delta\boldsymbol{\Gamma}|$ of the Lyapunov vector diverges exponentially in time. The dynamics given by Eqs. (B14), (B15), (B21), and (B22) shows that the divergence of $|\delta\boldsymbol{\Gamma}|$ must come from the Lyapunov vector components corresponding to colliding particles, as the other Lyapunov vector components diverge at most linearly. For this reason we neglect the change of the Lyapunov vector components for noncolliding particles. Under this assumption the Lyapunov vector dynamics for the Lyapunov vector component $\delta\boldsymbol{\Gamma}_l \equiv (\delta \boldsymbol{q}_l, \delta \boldsymbol{p}_l)^T$ for the lth particle is summarized as

$$\delta\boldsymbol{\Gamma}_j(t_n^+) \sim -\delta\boldsymbol{\Gamma}_k(t_n^+) \sim \tau_n \delta\boldsymbol{\Xi}^{[n-1]}, \tag{B23}$$

$$\delta\boldsymbol{\Gamma}_l(t_n^+) \sim \delta\boldsymbol{\Gamma}_l(t_{n-1}^+) \quad \text{for } l \notin \{j,k\}, \tag{B24}$$

where $\delta\boldsymbol{\Xi}^{[n-1]}$ is defined by

$$\delta\boldsymbol{\Xi}^{[n-1]} \equiv \begin{pmatrix} \mathcal{R}^{[n]} \delta \boldsymbol{p}_{k,j}(t_{n-1}^+) \\ \mathcal{Q}^{[n]} \delta \boldsymbol{p}_{k,j}(t_{n-1}^+) \end{pmatrix}. \tag{B25}$$

It is essential to note that the Lyapunov vector components $\delta\boldsymbol{\Gamma}_j(t_n^+)$ and $\delta\boldsymbol{\Gamma}_k(t_n^+)$ for the colliding particles have the same amplitude, and $\delta\boldsymbol{\Xi}^{[n-1]}$ is independent of τ_n.

We assume that the ratio

$$\nu \equiv \frac{|\delta \boldsymbol{q}_l|}{|\delta \boldsymbol{p}_l|} \tag{B26}$$

between the amplitudes of the spatial and momentum parts of the Lyapunov vector for the lth particle are independent of the particle index l [52]. Reference [29] suggests that the ratio ν need not be of order 1 in general. From Eq. (B26) we have

$$|\delta \boldsymbol{p}_l| \approx \frac{1}{\sqrt{1+\nu^2}} |\delta\boldsymbol{\Gamma}_l|. \tag{B27}$$

Using this assumption we estimate the magnitude of the vector $\delta\boldsymbol{\Xi}^{[n-1]}$ as

$$\begin{aligned} |\delta\boldsymbol{\Xi}^{[n-1]}| &= \max\{|\delta \boldsymbol{p}_j(t_{n-1}^+)|, |\delta \boldsymbol{p}_k(t_{n-1}^+)|\} \\ &\quad \times \sqrt{|\mathcal{R}^{[n]} \boldsymbol{e}^{[n]}|^2 + |\mathcal{Q}^{[n]} \boldsymbol{e}^{[n]}|^2} \\ &\approx \max\{|\delta\boldsymbol{\Gamma}_j(t_{n-1}^+)|, |\delta\boldsymbol{\Gamma}_k(t_{n-1}^+)|\} \\ &\quad \times \sqrt{\frac{|\mathcal{R}^{[n]} \boldsymbol{e}^{[n]}|^2 + |\mathcal{Q}^{[n]} \boldsymbol{e}^{[n]}|^2}{1+\nu^2}}, \end{aligned} \tag{B28}$$

where $\boldsymbol{e}^{[n]}$ is defined by

$$\boldsymbol{e}^{[n]} \equiv \frac{\delta \boldsymbol{p}_k(t_{n-1}^+) - \delta \boldsymbol{p}_j(t_{n-1}^+)}{\max\{|\delta \boldsymbol{p}_k(t_{n-1}^+)|, |\delta \boldsymbol{p}_j(t_{n-1}^+)|\}}, \tag{B29}$$

and satisfies the inequality

$$|\boldsymbol{e}^{[n]}| \leqslant \frac{|\delta \boldsymbol{p}_k(t_{n-1}^+)| + |\delta \boldsymbol{p}_j(t_{n-1}^+)|}{\max\{|\delta \boldsymbol{p}_k(t_{n-1}^+)|, |\delta \boldsymbol{p}_j(t_{n-1}^+)|\}} \leqslant 2. \tag{B30}$$

From Eq. (B28) we can estimate the magnitudes $|\delta \boldsymbol{\Gamma}_j(t_n^+)|$ and $|\delta \boldsymbol{\Gamma}_k(t_n^+)|$ through $|\delta \boldsymbol{\Gamma}_j(t_n^+)| = |\delta \boldsymbol{\Gamma}_k(t_n^+)| = \tau_n |\delta \boldsymbol{\Xi}^{[n-1]}|$.

Now, we introduce the clock value $\mathcal{K}_l(n)$ of the lth particle just after the nth collision as

$$\mathcal{K}_l(n) \equiv -\frac{1}{\ln \rho} \ln \frac{|\delta \boldsymbol{\Gamma}_l(t_n^+)|}{|\delta \boldsymbol{\Gamma}_l(0)|}, \tag{B31}$$

or equivalently, $|\delta \boldsymbol{\Gamma}_l(t_n^+)| = (1/\rho)^{\mathcal{K}_l(n)} |\delta \boldsymbol{\Gamma}_l(0)|$ leading to Eq. (6). Here ρ is the particle density whose value is $0 < \rho < 1$, and $\delta \boldsymbol{\Gamma}_l(0)$ is the Lyapunov vector component for the lth particle at the initial time. We choose the initial Lyapunov vector $\delta \boldsymbol{\Gamma}(0)$ so that its components $\delta \boldsymbol{\Gamma}_1(0), \delta \boldsymbol{\Gamma}_2(0), \ldots, \delta \boldsymbol{\Gamma}_{N-1}(0)$ and $\delta \boldsymbol{\Gamma}_N(0)$ have the same order of magnitude, and a larger clock value means larger magnitude of the Lyapunov vector component, $|\delta \boldsymbol{\Gamma}_l(t_n)|$.

We have already used the fact that the free-flight time increases as the density ρ decreases. To write down the clock value more meaningfully, we use the specific relation between the free-flight time and the density, namely that the free-flight time $\tau_n M$ is approximately inversely proportional to the density ρ at low density;

$$\tau_n \sim s_n/\rho, \tag{B32}$$

where s_n is independent of the density. Using Eq. (B32), the expression (B31) for the clock value $\mathcal{K}_l(n)$ can be rewritten as

$$\mathcal{K}_l(n) \sim \begin{cases} \max\{\mathcal{K}_j(n-1), \mathcal{K}_k(n-1)\} + 1 + \Delta\Phi^{[n]} & \text{for } l = j \text{ or } l = k, \\ \mathcal{K}_l(n-1) & \text{for } l \notin \{j,k\}, \end{cases} \tag{B33}$$

where $\Delta\Phi^{[n]}$ is defined by

$$\Delta\Phi^{[n]} \equiv -\frac{1}{\ln \rho} \ln \left\{ s_n \sqrt{\frac{|\mathcal{R}^{[n]} \boldsymbol{e}^{[n]}|^2 + |\mathcal{Q}^{[n]} \boldsymbol{e}^{[n]}|^2}{1+\nu^2}} \right\}, \tag{B34}$$

and where we have used Eqs. (B23), (B28), and (B31), and $|\delta \boldsymbol{\Gamma}_j(0)| \approx |\delta \boldsymbol{\Gamma}_k(0)|$. Our final assumption to derive the clock model is that

$$\lim_{\rho \to 0} \Delta\Phi^{[n]} = 0. \tag{B35}$$

To justify the assumption (B35) note that the right-hand side of Eq. (B34) for the quantity $\Delta\Phi^{[n]}$ has a factor $1/\ln \rho$ which goes to zero in the limit as $\rho \to 0$, and s_n, $\mathcal{Q}^{[n]}$, and $\mathcal{R}^{[n]}$ are almost independent of the density ρ, and the magnitude of the vector $\boldsymbol{e}^{[n]}$ is finite even in the limit $\rho \to 0$ from the inequality (B30) [52]. Equations (B33) and (B35) lead to the clock dynamics

$$\mathcal{K}_l(n) \sim \begin{cases} \max\{\mathcal{K}_j(n-1), \mathcal{K}_k(n-1)\} + 1 & \text{for } l = j \text{ or } l = k, \\ \mathcal{K}_l(n-1) & \text{for } l \notin \{j,k\}, \end{cases} \tag{B36}$$

in the low density limit, which is closed by the clock value $\mathcal{K}_l(n)$ only, except for determining the indices j and k of colliding particles. From Eq. (B36), the dynamics for the clock model is expressed as (i) the clock value is changed only when the corresponding particle collides, and (ii) the clock values of colliding particles are tuned to the same value given by 1 plus the larger of the two clock values of the particles just before the collision.

In the quasi-one-dimensional system with periodic boundary conditions the colliding particles can be taken to be j and $k = j+1$ (note that index $N+1$ is equivalent to 1). Therefore we obtain the dynamics (5) for the brick accumulation model explained in Sec. IV as the one-dimensional version of the clock model. Moreover, in the one-dimensional case, $\mathcal{K}_l(n)$ can be interpreted as the brick height of the l-site just after the nth brick is dropped.

Finally we derive formula (7) for the largest Lyapunov exponent from the clock value $\mathcal{K}_l(n)$. In the limit of low density $\rho \ll 1$, the amplitude $|\delta \boldsymbol{\Gamma}(t_n^+)|$ of the Lyapunov vector can be approximated by

$$|\delta \boldsymbol{\Gamma}(t_n^+)| = \sqrt{\sum_{l=1}^{N} |\delta \boldsymbol{\Gamma}_l(t_n^+)|^2} \sim \alpha_n \left(\frac{1}{\rho}\right)^{\tilde{\mathcal{K}}^{[\max]}(n)} |\delta \boldsymbol{\Gamma}_l(0)| \tag{B37}$$

noting that the sum $\Sigma_{l=1}^{N} |\delta \boldsymbol{\Gamma}_l(t_n^+)|^2$ is dominated by the Lyapunov vector component amplitude $|\delta \boldsymbol{\Gamma}_l(t_n^+)|$ with the largest clock value $\tilde{\mathcal{K}}^{[\max]}(n) \equiv \max\{\mathcal{K}_1(n), \mathcal{K}_2(n), \ldots, \mathcal{K}_N(n)\}$

at n, because of the huge factor $1/\rho$. Here, α_n is the number of particles with the largest clock value $\tilde{\mathcal{K}}^{[\max]}(n)$, and we have also used our assumption that $|\delta\mathbf{\Gamma}_l(0)|$ is almost independent of the particle index l. Now we assume the approximate relation

$$\frac{\tilde{\mathcal{K}}^{[\max]}(n)}{n} \overset{n\to\infty}{\sim} \frac{1}{nN}\sum_{l=1}^{N} \mathcal{K}_l(n) \tag{B38}$$

in the limit of large n. (We have checked this relation numerically for the brick accumulation model.) Using the relations (B37) and (B38), and $t \sim n\tau$ we obtaine

$$\lambda \equiv \lim_{t\to+\infty} \frac{1}{t} \ln|\delta\mathbf{\Gamma}(t)| \sim -\lim_{n\to+\infty} \frac{1}{n\tau}\tilde{\mathcal{K}}^{[\max]}(n)\ln\rho$$

$$\sim -\lim_{n\to+\infty} \frac{1}{n\tau N}\sum_{l=1}^{N} \mathcal{K}_l(n)\ln\rho \tag{B39}$$

for the Lyapunov exponent λ corresponding to the Lyapunov vector $\delta\mathbf{\Gamma}$. Therefore we obtain Eq. (7), which is independent of the system shape and the number of spatial dimensions.

[1] D. J. Evans and G. P. Morriss, *Statistical Mechanics of Nonequilibrium Liquids* (Academic Press, London, 1990).
[2] P. Gaspard, *Chaos, Scattering and Statistical Mechanics* (Cambridge University Press, Cambridge, England, 1998).
[3] J. R. Dorfman, *An Introduction to Chaos in Nonequilibrium Statistical Mechanics* (Cambridge University Press, Cambridge, England, 1999).
[4] U. Dressler, Phys. Rev. A **38**, 2103 (1988).
[5] D. J. Evans, E. G. D. Cohen, and G. P. Morriss, Phys. Rev. A **42**, 5990 (1990).
[6] C. P. Dettmann and G. P. Morriss, Phys. Rev. E **53**, R5545 (1996).
[7] T. Taniguchi and G. P. Morriss, Phys. Rev. E **66**, 066203 (2002).
[8] J.-P. Eckmann and D. Ruelle, Rev. Mod. Phys. **57**, 617 (1985).
[9] J.-P. Eckmann and I. Procaccia, Phys. Rev. A **34**, 659 (1986).
[10] P. Cvitanović, R. Artuso, R. Mainieri, G. Tanner, and G. Vattay, *Chaos: Classical and Quantum*, ChaosBook.org (Niels Bohr Institute, Copenhagen, 2005).
[11] D. J. Evans, E. G. D. Cohen, and G. P. Morriss, Phys. Rev. Lett. **71**, 2401 (1993).
[12] G. Gallavotti and E. G. D. Cohen, Phys. Rev. Lett. **74**, 2694 (1995).
[13] D. J. Evans and D. J. Searles, Adv. Phys. **51**, 1529 (2002).
[14] H. A. Posch and R. Hirschl, in *Hard Ball Systems and the Lorentz Gas*, edited by D. Szász (Springer, Berlin, 2000), p. 279.
[15] T. Taniguchi and G. P. Morriss, Phys. Rev. E **65**, 056202 (2002).
[16] A. S. de Wijn and H. van Beijeren, Phys. Rev. E **70**, 016207 (2004).
[17] H. L. Yang and G. Radons, Phys. Rev. E **71**, 036211 (2005).
[18] T. Taniguchi and G. P. Morriss, Phys. Rev. E **68**, 026218 (2003).
[19] T. Taniguchi and G. P. Morriss, Phys. Rev. E **71**, 016218 (2005).
[20] J.-P. Eckmann, C. Forster, H. A. Posch, and E. Zabey, J. Stat. Phys. **118**, 813 (2005).
[21] T. Taniguchi and G. P. Morriss, Phys. Rev. Lett. **94**, 154101 (2005).
[22] P. Manneville, Lect. Notes Phys. **230**, 319 (1985).
[23] K. Kaneko, Physica D **23**, 436 (1986).
[24] R. Livi and S. Ruffo, in *Nonlinear Dynamics*, edited by G. Turchetti (World Scientific, Singapore, 1989), p. 220.
[25] M. Falcioni, U. M. Marconi, and A. Vulpiani, Phys. Rev. A **44**, 2263 (1991).
[26] T. Dauxois, S. Ruffo, and A. Torcini, Phys. Rev. E **56**, R6229 (1997).
[27] A. Pikovsky and A. Politi, Phys. Rev. E **63**, 036207 (2001).
[28] Lj. Milanović and H. A. Posch, J. Mol. Liq. **96–97**, 221 (2002).
[29] T. Taniguchi and G. P. Morriss, Phys. Rev. E **68**, 046203 (2003).
[30] C. M. Newman, Commun. Math. Phys. **103**, 121 (1986).
[31] J.-P. Eckmann and C. E. Wayne, J. Stat. Phys. **50**, 853 (1988).
[32] T. Taniguchi, C. P. Dettmann, and G. P. Morriss, J. Stat. Phys. **109**, 747 (2002).
[33] L. Casetti, R. Livi, and M. Pettini, Phys. Rev. Lett. **74**, 375 (1995).
[34] L. Casetti, M. Pettini, and E. G. D. Cohen, Phys. Rep. **337**, 237 (2000).
[35] R. van Zon, H. van Beijeren, and Ch. Dellago, Phys. Rev. Lett. **80**, 2035 (1998).
[36] R. van Zon, H. van Beijeren, and J. R. Dorfman, in *Hard Ball Systems and the Lorentz Gas*, edited by D. Szász (Springer, Berlin, 2000), p. 231.
[37] R. van Zon and H. van Beijeren, J. Stat. Phys. **109**, 641 (2002).
[38] T. Taniguchi and G. P. Morriss, e-print nlin.CD/0502032.
[39] C. Forster and H. A. Posch, New J. Phys. **7**, 32 (2005).
[40] Ch. Forster, D. Mukamel, and H. A. Posch, Phys. Rev. E **69**, 066124 (2004).
[41] G. Benettin, L. Galgani, and J.-M. Strelcyn, Phys. Rev. A **14**, 2338 (1976).
[42] I. Shimada and T. Nagashima, Prog. Theor. Phys. **61**, 1605 (1979).
[43] G. Benettin, L. Galgani, A. Giorgilli, and J.-M. Strelcyn, Meccanica **15**, 9 (1980).
[44] G. Benettin, L. Galgani, A. Giorgilli, and J.-M. Strelcyn, Meccanica **15**, 21 (1980).
[45] Ch. Dellago, H. A. Posch, and W. G. Hoover, Phys. Rev. E **53**, 1485 (1996).
[46] L. Frachebourg, Ph. A. Martin, and J. Piasecki, Physica A **279**, 69 (2000).
[47] F. Romá, C. M. Horowitz, and E. V. Albano, Phys. Rev. E **66**, 066115 (2002).
[48] G. Giacomelli and A. Politi, Europhys. Lett. **15**, 387 (1991).
[49] A. Pikovsky and A. Politi, Nonlinearity **11**, 1049 (1998).

[50] In the actual simulation of the brick accumulation model we discarded the brick accumulations after the first $100N$ bricks have been dropped. Thus the sum $\Sigma_{j=1}^{N}\mathcal{K}_j(n)$ is not zero at $n=0$. This is the reason why we added the fitting parameter ξ in the function $\Sigma_{j=1}^{N}\mathcal{K}_j(n)=\xi+\omega n$ in Fig. 6 although it is almost zero in this case.

[51] More exactly, the distribution $D(\boldsymbol{\sigma}\cdot\Delta\boldsymbol{p})$ for nonzero hopping cases in Fig. 10 was calculated as follows. First we chose the case satisfying the conditions: (i) the particle indices satisfying $\gamma_j^{(1)}>0.2$ are given by $\{j_n,j_n+1\}$ just before the nth collision and $\{j_{n+1},j_{n+1}+1\}$ just after the nth collision, such that $j_n \neq j_{n+1}$, and (ii) the j_{n+1}th particle and $(j_{n+1}+1)$th particle collide at the nth collision. (Here, if the particle indices for the localized region of the Lyapunov vector satisfy $\gamma_j^{(1)}>0.2$ is $\{1,N\}$, then the particle indices pair $\{j_n,j_n+1\}$ or $\{j_{n+1},j_{n+1}+1\}$ above should be taken as $\{0,1\}$, based on periodic boundary conditions.) Then we calculate the distribution $D(\boldsymbol{\sigma}\cdot\Delta\boldsymbol{p})$ from the value of $\boldsymbol{\sigma}\cdot\Delta\boldsymbol{p}$ in the nth collision between these j_{n+1}th and $(j_{n+1}+1)$th particles.

[52] Reference [29] suggests that the ratio ν depends on the density ρ, and it can be $\nu\gg 1$ for a Lyapunov vector corresponding to a positive Lyapunov exponent at low density. Therefore the assumption (B35) is not obvious.